DocumentID: 370214

VALIDATING GLOBAL STRUCTURAL DAMPING MODELS FOR DYNAMIC ANALYSES

M. Höser * , M. Böswald ** , Y. Govers **

* Technische Universität Berlin, Institut für Luft- und Raumfahrt, Marchstr. 12-14, 10587 Berlin, Germany

** Deutsches Zentrum für Luft- und Raumfahrt e.V., Institut für Aeroelastik, Bunsenstr. 10, 37073 Göttingen, Germany

Abstract:

Finite Element (FE) models grow in terms of detail and complexity. They strive to provide a more precise mass and stiffness distribution in order to achieve better load prediction capabilities. However, they also need to include damping models to achieve better results for dynamic loads analyses. This is why experiments are usually carried out to quantify global damping ratios of the final structure and include them in the analytical model for further calculations. Yet, especially for large aerospace structures assembled from different substructures, the experimental determination of damping ratios for the assembled structure may be impossible or ineconomical. Therefore, a consistent approach to predict the damping properties of assembled structures is desirable.

In this work, FE models of a laboratory test structure and its two substructures are built up. Modal tests are carried out on the substructures. On the basis of correlated substructure modal damping ratios, global proportional damping models are applied on substructure level in order to build proportional substructure damping matrices, construct a nonproportional, full structure damping matrix and thus predict the damping properties for the fully assembled structure. The approach is validated with the help of experimental results from a modal test on the fully assembled laboratory test structure.

Because of the unsatisfactory reproduction of the substructure damping properties by the selected damping models and the outcome for the assembled structure in this work, an additional investigation on computational model updating of damping parameters on substructure level is carried out on a simulated plate.

Keywords: Structural Dynamics, Damping Prediction, Modal Analysis, Substructure Damping, Model Updating

1. INTRODUCTION

Vibrations are commonly met in structures in aerospace, as well as civil and mechanical engineering, as a result of complex dynamic loads. They contribute to a decrease in fatigue life and can lead to functional failure of these structures. Their properties need to be determined and included in analytical models in order to guarantee a safe and economical structural design and allow further modelling of complex external and system-dependent loads at a preliminary stage of development.

Finite Element Analysis (FEA) procedures are extensively used for the analysis of structures and the analytical calculation of dynamic structural properties. For their application, the structure is discretised into a set of finite elements with mass and stiffness properties.

Due to the steady performance improvements of computational systems, FE models tend to grow especially in terms of a finer structural discretisation to improve the prediction capabilities of the model. However, they usually do not include damping.

Damping is an important attribute in the sense that it balances external forces, limits resonance peaks of steady-state long-term responses and leads to a more rapid decay of free vibrations after transient loadings. Its inclusion would therefore improve the quality of analytical models immensely. Yet, it is the most uncertain attribute in structural dynamics, because the locations and causes of energy dissipation in a structure are very hard to predict theoretically. For this reason, it is common practise to determine damping properties on a global level of the final structure in experiments first and include it as modal damping ratios in analytical models after that.

Experimental Modal Analysis (EMA) is used as a system identification tool to determine the modal properties of a real structure from vibration measurement data and to validate FE models. Damping properties of a structure can be determined with a reasonable accuracy if the testing and data processing are performed in a careful way.

With respect to large complex aerospace structures assembled from many components, there are two challenges:

- EMA cannot be carried out because the system is too large to excite and to measure vibration responses, or because of economical constraints.
- If damping properties from experiments are available for the assembled system, proportional damping models usually fail to reflect the cause and location of damping in the assembled structure because the actual damping patterns due to different materials and substructures are unknown.

As an approach, global proportional damping models on the basis of experimental results of substructures are developed. They are applied to the substructure FE models to generate uncondensed substructure damping matrices which are then coupled to represent an uncondensed nonproportional damping matrix of the fully assembled structure. This work investigates how well this approach predicts the damping properties of the assembled structure. A laboratory test structure which can be disassembled is available for experimental validation.

Four global proportional damping models were selected for this investigation.

- Classic RAYLEIGH damping is a commonly used textbook model.
- Viscous modal damping is state-of-the-art but led to severe errors in past response analysis studies with coupled substructures, e.g. in [1].
- Stiffness proportional structural damping is a newer textbook model which is part of the *Equivalent Structural Damping* (ESD) concept applied in [1]. There, it achieved more consistent results than constant viscous modal damping for coupled dynamic loads analyses.
- Structural modal damping is another model presented as part of the ESD concept, but is not studied further in [1].

Because the explained approach does not lead to satisfactory results in the course of this article, a computational model updating process is later introduced on the basis of complex eigenvalue sensitivity matrices of damped systems, studied in [2]. This is done in order to improve the agreement of substructure damping properties derived from experiments with analytically calculated properties and, in the future, to better reproduce the damping properties of an assembled structure.

2. GLOBAL DAMPING MODELS

The second-order differential equations of motion for free undamped vibration of a structure, modelled as a discrete multi-degree-of-freedom (MDOF) system with n degrees of freedom (DOF), can be written as

$$[M]\{\ddot{u}(t)\} + [K]\{u(t)\} = \{0\} \tag{1}$$

where $[M]$ and $[K] \in \mathbb{R}^{n\times n}$ are the symmetric system mass and stiffness matrices and $\{u(t)\}$ is the time-dependent DOF displacement vector. The solution of the eigenvalue problem leads to n pairs of complex conjugated eigenvalues $\lambda_{n1/n2} = \pm i\omega_{0,n}$, containing the natural undamped frequency $\omega_{0,n}$, and n real eigenvectors $\{\phi_n\} \in \mathbb{R}^{n\times 1}$.

Damping is a structural attribute that makes energy dissipate out of the vibrating system due to irreversible processes and transforms it into heat. Internal damping depends on the material, the temperature, the type of loading and the vibration frequency and originates from within the structure. This type of damping can be modelled by *global* damping models. Damping can also result from the layout of the structural assembly leading to friction at contact areas. This type of damping can be modelled by *local* damping models.

It is commonly accepted that damping effects are stronger at local contact areas. But as a starting point, *global* proportional damping models which represent internal system damping processes are investigated to set a good foundation for further *local* damping modelling.

2.1 RAYLEIGH damping

RAYLEIGH damping is a combination of stiffness proportional viscous (s,v) and mass proportional viscous (m,v) damping and results in the symmetric viscous system damping matrix $[D] \in \mathbb{R}^{n\times n}$ for FE MDOF systems.

$$[D] = g_{m,v}[M] + g_{s,v}[K] \tag{2}$$

The equations of motion for free viscously damped vibration of a structure are then given by

$$[M]\{\ddot{u}(t)\} + [D]\{\dot{u}(t)\} + [K]\{u(t)\} = \{0\} \tag{3}$$

The solution of the eigenvalue problem which has to be formulated in state-space results in n pairs of complex conjugated eigenvalues $\lambda_{n1/n2} = -D_n\omega_{0,n} \pm i\omega_{0,n}\sqrt{1-D_n^2}$. Due to the linear dependency of $[D]$ on $[M]$ and $[K]$, the resulting eigenvectors $\{\phi_n\}$ are the same as for the undamped system and orthogonal to $[D]$. Modal decoupling leads to generalised damping constants d_{gen} and a combined linear and hyperbolic dependency of the n-th modal damping ratio D_n on the n-th natural undamped frequency $\omega_{0,n}$.

$$D_n = \frac{1}{2}g_{s,v}\omega_{0,n} + \frac{1}{2}g_{m,v}\frac{1}{\omega_{0,n}} \tag{4}$$

2.2 Stiffness proportional structural damping

Viscoelastic behaviour often is an inadequate assumption for the internal damping of ductile elastic materials like metal and steel concrete. Instead, the energy dissipation per cycle, which is described as the damping ratio D, has been shown to be almost independent from the forcing frequency Ω for harmonic

forced vibrations. This behaviour is approximated by substituting the loss factor $g_{s,v}$ in the viscous stiffness proportional damping model with

$$g_{s,v} = \frac{g_{s,s}}{\Omega} \tag{5}$$

This model is only valid for stationary harmonic vibrations at a frequency Ω and therefore only in the frequency domain. Non-harmonic dynamic loads lead to non-causal behaviour in the time domain.

Assuming that the loaded structure responds with $\{u(t)\} = \{\hat{u}\}e^{i\omega t}$ with $\omega = \Omega$, the modal damping ratio is constant.

$$D = \frac{1}{2} g_{s,s} \frac{\omega}{\Omega} \approx \frac{1}{2} g_{s,s} = \text{const} \tag{6}$$

The equations of motion change to

$$[M]\{\ddot{u}(t)\} + [K^c]\{u(t)\} = \{0\} \tag{7}$$

where the system stiffness matrix $[K^c] \in \mathbb{C}$ is $[K^c] = [K](1+ig_{s,s}) = [K]+i[C]$. The solution of the complex eigenvalue problem is still possible and gives n pairs of complex eigenvalues $\lambda_{n1/n2} = \pm i\omega_{0,n}\sqrt{1+i2D_n}$. Due to the stiffness proportionality of $[C]$, the n eigenvectors $\{\phi_n\}$ are the same as for the undamped neighbouring system.

2.3 Modal damping

For *viscoelastic* behaviour, a modally decoupled, therefore diagonal generalised damping matrix $[D]_{gen} \in \mathbb{R}^{h\times h}$ can be built out of the h chosen modal damping ratios D_h for the first h structural modes of the undamped FE MDOF system

$$[D]_{gen} = [\Phi]^{\mathsf{T}}[D][\Phi] = \begin{bmatrix} d_{gen,1} & 0 & 0 & 0 \\ 0 & d_{gen,2} & 0 & 0 \\ \vdots & & \ddots & \\ 0 & 0 & 0 & d_{gen,h} \end{bmatrix} \tag{8}$$

where $d_{gen,h} = 2D_h\omega_{0,h}m_{gen,h}$ is the generalised damping constant of mode h and the modal matrix $[\Phi] \in \mathbb{R}^{h\times n}$ contains the first h real structural modes $\{\phi\}_h$ of the neighbouring undamped system.

In case of a modal system with exclusively generalised DOFs $q_h(t)$, $[D]_{gen}$ can be transformed to the corresponding viscous damping matrix $[D]$ with the modal synthesis

$$[D] = [M]\left(\sum_1^h \frac{2D_h\omega_{0,h}}{m_{gen,h}}\{\phi_h\}\{\phi_h\}^{\mathsf{T}}\right)[M] \tag{9}$$

For *structural* behaviour, a modally decoupled generalised damping matrix $[C]_{gen} \in \mathbb{R}^{h\times h}$ is built from the h chosen modal damping ratios D_h for the first h structural modes of the undamped FE MDOF system

$$[C]_{gen} = [\Phi]^{\mathsf{T}}[C][\Phi] = \begin{bmatrix} c_{gen,1} & 0 & 0 & 0 \\ 0 & c_{gen,2} & 0 & 0 \\ \vdots & & \ddots & \\ 0 & 0 & 0 & c_{gen,h} \end{bmatrix} \tag{10}$$

where the imaginary generalised stiffness $c_{gen,h} = 2D_hk_{gen,h}$ is part of the generalised complex stiffness $k^c_{gen,h} = k_{gen,h} + ic_{gen,h}$ [1].

The corresponding imaginary part of the complex stiffness system matrix $[C]$ can be acquired by using

$$[C] = [M]\left(\sum_1^h \frac{2D_h\omega_{0,h}^2}{m_{gen,h}}\{\phi_h\}\{\phi_h\}^{\mathsf{T}}\right)[M] \tag{11}$$

Both uncondensed modal damping matrices $[D]$ and $[C]$ are proportional and are rank-deficient with a rank $h \ll n$. Additionally, both behave *equivalently* at the peak resonances and therefore yield the same modal damping ratios, but behave differently for steady-state harmonic loads with forcing frequencies in between the resonant frequencies. Plus, the uncondensed damping matrices are fully populated and therefore cause significant numerical effort on computer systems for FE models with a high number of DOFs.

A very important difference of modal damping in comparison to damping models in section 2.1 and section 2.2 is that modal damping distributes damping in the structure only with respect to the target modal damping ratios of specific mode shapes at specific frequencies. Because of this intransparent distribution, it does not give any clues as to how or where damping is located in the structure. Additionally, only those h modes which are assigned a modal damping ratio D_h are damped, the others are undamped. For these reasons, an uncondensed damping matrix is not truly physical because it relies on mathematics and the system specifications. Consequently, a change of constraints or interfaces or a coupling procedure may lead to different mode shapes and frequencies, resulting in strongly divergent modal damping ratios, a phenomenon known as damping paradox [1].

2.4 Nonproportional damping

As noted in section 1, experimental modal damping ratios of the full structure may not be available so that modal damping is not an option. If, in addition, the mechanical system consists of different materials, elements or substructures with individual energy dissipation behaviours, its damping pattern can most probably not be approximated by proportional damping models based on just one or two loss factors g in a satisfying manner.

However, one approach can be the application of global proportional damping models to the substructures of the system on the basis of experimental data of the substructures. Coupling of the substructure pro-

portional damping matrices results in a system damping matrix $[D]$ or $[C]$ which is nonproportional with respect to the full coupled system.

With nonproportional damping, the solution of the eigenvalue problem of viscously damped, nonproportional systems leads to n complex conjugated pairs of eigenvectors $\{\psi\}_{n1/n2}$. The solution of structurally damped, nonproportional systems is characterised by n complex eigenvectors $\{\psi\}_n$.

3. TEST BED MODELLING AND TESTING

The test structure "Aircraft Model" (AIRMOD) of the DLR Göttingen is an almost identical duplicate of the test bed which was investigated in a multinational EMA study performed by the Group for Aeronautical Research and Technology in Europe (GARTEUR), department Structures and Materials, Action Group 19 (SM-AG19) [3][4].

It consists of strictly rectangular aluminum plates and beams connected by bolted joints and has the simplified shape of a conventional fixed-wing aircraft. It has a length of 1.5 m, a wingspan of 2 m and a height of 0.46 m. The most notable difference of the DLR test bed in comparison to the GARTEUR test bed is the absence of the constrained-layer damping treatment applied to the wing of the GARTEUR model. FIG. 1 shows a sketch of AIRMOD on the left side.

The connection box which is located at the joint of the wing and the fuselage consists of two thin aluminum plates joined together by 4 screws. At this location, it is simple to split up the AIRMOD into two substructures: the wing (including the upper connection box plate and the two winglets) and the fuselage (including the lower connection box plate and the vertical and horizontal tailplanes).

AIRMOD has been tested several times in the frequency range between 0 and 400 Hz, but was retested on the basis of recent results in [5] and [6] because of a newly built support frame and the strong sensitivity of modal damping properties.

The identified modal damping ratios of the two substructures are intended as a basis to model substructure damping according to the damping models in section 2. The identified damping ratios of the full structure are intended for comparison against the numerically calculated modal damping ratios from the solution of the eigenvalue problem of the full structure with coupled damped substructures.

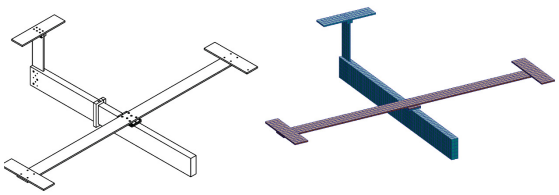

FIG 1. Sketch of AIRMOD (left), full structure FE model without suspension (right)

Modal damping ratios D_n are unique for the corresponding mode shapes $\{\psi\}_n$. Thus, if modal damping ratios of the substructures are used to model and predict the dynamic behaviour of the full structure, the mode shapes of the substructure in test conditions should very well match the mode shapes of the substructure when coupled.

Therefore, the full structure was modelled and tested in a free condition. To achieve a state of suspension which has almost no influence on the elastic modes, AIRMOD was hung into a support frame using soft bungee cords.

The substructures were modelled and tested while being fixed at their interfaces. For clamped boundary conditions, an air-cushioned seismic foundation was available.

3.1 Finite Element Modelling

An MSC.NASTRAN FE model of AIRMOD was made available where the original element type choices were reviewed to avoid idealisation errors.

All of the aluminum components are modelled by CHEXA solid elements. The elasticity of the screws used for component connections and clamping of the substructures are modelled as multiple CELAS1 scalar springs located at at coincident nodes of the adjacent component surfaces, in all three translational directions. CONM2 lumped mass elements comprise the masses of single elements which are fixed to the structure. Massless, pinned-end CBAR first-order bar elements model the elasticity of the bungee cords.

To verify the convergence properties of the FE models, an h-convergence analysis was conducted using natural frequencies. Due to the size of the FE model, the investigation was limited on half a wing which has the strongest influence on the AIRMOD modes.

The full structure FE model, also shown in FIG. 1, uses 1990 elements and 10075 nodes and has 30222 DOFs.

The substructure FE models originating from the full structure model have the same mesh, element and material properties as the full structure. In FIG. 1, the wing substructure is marked in red and the fuselage substructure is marked in blue colour.

3.2 Modal Testing

Modal data in the frequency range of interest between 0 and 400 Hz was gained from AIRMOD and its two substructures by means of experimental modal analysis (EMA).

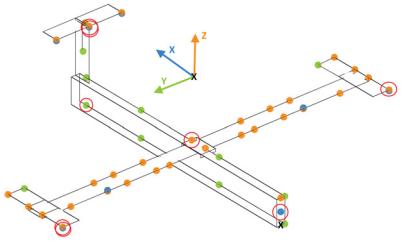

FIG 2. Sensor locations and directions (as blue, green, orange dots), driving point locations (as red circles)

The phase separation method was applied by means of impulse excitation with a modal hammer. Each acceleration sensor weighed 2 g.

50 uniaxial sensor locations were selected for the full structure. The wing carried 32 sensors and the fuselage 18 sensors. The locations are shown in FIG. 2 for the full structure.

8 driving point locations in total, 4 on the wing and 4 on the fuselage, were selected in and beyond the symmetry planes of AIRMOD in order to excite symmetric as well as antisymmetric mode shapes. They were chosen according to the occurrence of large vibration amplitudes expected by the preliminary FE models. They are also shown in FIG. 2 as red circles around the corresponding sensors. At least three up to five out of the 8 different locations were used for full structure and substructure tests.

The modal test setups are shown in FIG. 3 and FIG. 4.

For the processing of the acquired FRFs and the identification of modes and their properties, the Poly-Reference Least-Squares Complex Frequency Domain (pLSCF) method, also known as PolyMAX, was employed [7].

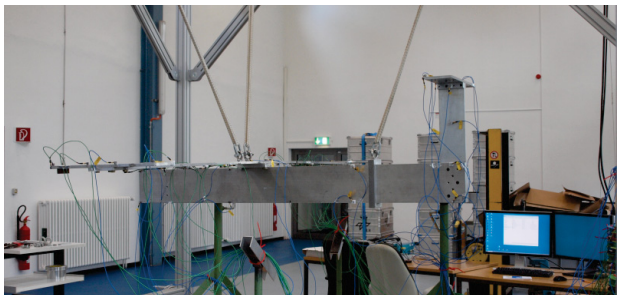

FIG 3. Experimental setup of the fully assembled AIRMOD

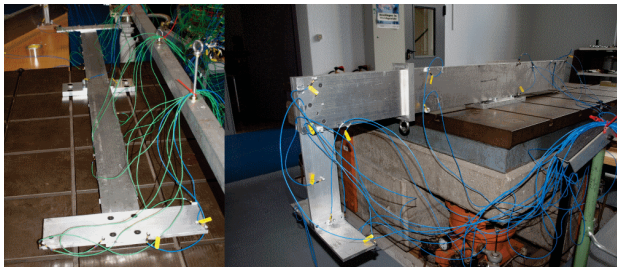

FIG 4. Experimental setups of wing (left) and fuselage (right)

The identified modes and their properties were evaluated by using quality indicators, especially the Modal Phase Collinearity (MPC) criterion, the Mean Phase Deviation (MPD) criterion, the phase of the modal a $a_{gen} \in \mathbb{C}$, and the generalised mass m_{gen}, with the aid of the DLR in-house software *Correlation Tool*. This process enables a classification of the reliability of identified modes and eigenvalues and ensures that the resulting modal models of the 3 test cases represent the respective dynamic behaviour with good accuracy. These modal test results are used for model validation.

The modal properties and some quality criteria values of the first five and the last identified elastic modes of each test are listed in TAB. 1, TAB. 2 and TAB. 3.

For the wing substructure, 18 elastic modes were identified. Only one of them could not be identified well enough and was removed from further analyses.

For the fuselage substructure, 11 modes were identified, all of them in a high quality. Mode #3 at 49.34 Hz was a rigid body mode because of the elastic fixing between fuselage and baseplate and the high moment of inertia of the fuselage. Therefore, its modal damp-

Mode #	f_0 [Hz]	D_{gen} [%]	**MPC** [%]	**MPD** [°]	**Phase** a_{gen} [°]	m_{gen} [kgm^2]
1	5.15	0.26	98.33	5.49	-77.53	5.49
2	5.18	0.09	99.54	5.04	-69.84	1.97
3	33.33	0.16	100.00	0.12	-91.76	0.67
4	33.40	0.23	99.99	0.63	-90.29	0.58
5	43.93	0.27	99.43	4.16	-89.02	1.59
:	:	:	:	:	:	:
18	343.38	0.50	99.97	1.05	-84.07	1.12

TAB 1. Modal properties of wing elastic modes

Mode #	f_0 [Hz]	D_{gen} [%]	**MPC** [%]	**MPD** [°]	**Phase** a_{gen} [°]	m_{gen} [kgm^2]
1	25.08	0.48	99.98	0.79	-75.49	3.37
2	43.16	0.47	99.99	0.69	-86.95	3.08
4	68.11	0.41	100.00	0.34	-70.46	0.53
5	97.69	0.42	99.98	0.76	-77.22	3.70
6	108.39	1.12	100.00	0.25	-82.31	0.56
:	:	:	:	:	:	:
11	321.45	0.50	99.94	1.42	-86.82	5.14

TAB 2. Modal properties of fuselage elastic modes

Mode #	f_0 [Hz]	D_{gen} [%]	**MPC** [%]	**MPD** [°]	**Phase** a_{gen} [°]	m_{gen} [kgm^2]
5	5.52	0.36	100.00	0.31	-87.23	4.48
6	15.15	0.30	100.00	0.17	-88.40	4.37
7	32.73	0.28	99.75	2.87	-93.29	1.03
8	33.09	0.35	99.85	2.20	-92.95	0.93
9	34.99	0.44	99.97	1.07	-89.30	2.23
:	:	:	:	:	:	:
30	355.68	0.29	99.75	2.90	-87.93	10.43

TAB 3. Modal properties of AIRMOD elastic modes

ing ratio represents the damping from the mounting rather than from the structure.

For the fully assembled AIRMOD, 26 elastic modes were identified of which 2 showed an insufficient identification quality and had to be removed from further processing. 4 rigid body modes were identified in a frequency range of 0.42 up to 0.98 Hz.

In a first comparison to the experimental data, the FE models showed good agreement in terms of natural undamped frequencies and mode shape prediction of the elastic modes. They were further improved by accounting for the mass and positions of measurement equipment and adjusting the elasticity of the bolted joints.

The precise correlation of modal properties from the improved FE models and the experimental test data is necessary to check the validity of the FE models. For this reason, the linear independence among the analytical real mode shapes and the realised, weakly complex mode shapes from the modal tests were checked with the Modal Assurance Criterion (MAC) [8]

$$\text{MAC}_{jk} = \frac{\left(\{\phi_j\}^\intercal\{\phi_k\}\right)^2}{\left(\{\phi_j\}^\intercal\{\phi_j\}\right)\left(\{\phi_k\}^\intercal\{\phi_k\}\right)} \tag{12}$$

where MAC_{jk} is the normed scalar product of vectors $\{\phi_j\}$ and $\{\phi_k\}$ can take values between 1 for fully linearly dependent and 0 for linearly independent vectors.

The MAC matrix of the clamped fuselage structure is shown in FIG. 5, with the correlated modes framed in green. One example of correlated mode shapes is depicted in FIG. 6.

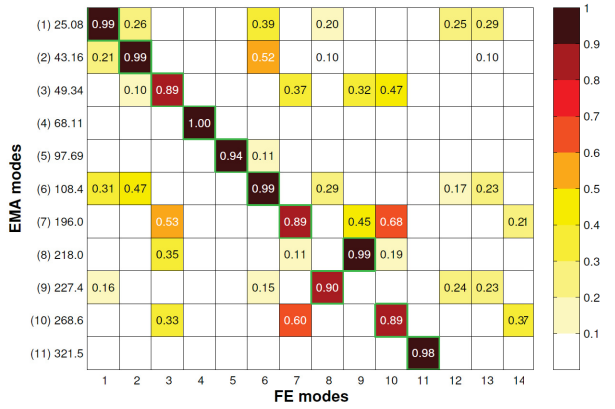

FIG 5. MAC matrix of fuselage structure FE and EMA data

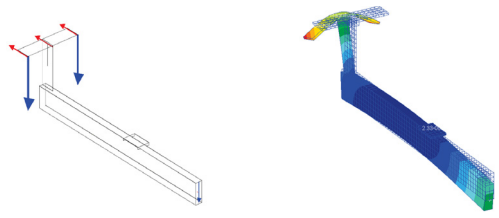

FIG 6. Mode shape of fuselage, EMA: 7, FE: 7 (MAC: 89%)

The correlation process resulted in allocating all numerically predicted elastic modes to experimentally identified modes.

4. DAMPING MATRIX COUPLING AND RESULTS

On the basis of experimental data and the correlated FE models of the substructures, the substructure damping will be modelled, coupled and fed to the eigenvalue problem of the full AIRMOD FE model.

MSC.NASTRAN is not used further in this process because the software package does not offer possiblities of allocating RAYLEIGH damping to confined FE areas without having to resort to superelements and the thereby mandatory CRAIG-BAMPTON condensation. Instead, the a-set substructure stiffness and mass matrices $[K]$ and $[M]$ are exported from the corresponding MSC.NASTRAN FE models and imported into MATLAB.

First, the substructure damping matrices $[D]$ are calculated with the help of the substructure system matrices and the experimental data.

In case of the RAYLEIGH damping, the loss factors $g_{m,v}$ and $g_{s,v}$ are estimated by fitting EQ. (4) to the experimental modal damping ratios with the aid of linear least squares. In case of stiffness proportional structural damping, the loss factor $g_{s,s}$ is estimated by calculating the doubled mean of the experimentally identified modal damping ratios, according to EQ. (6). Modal damping ratios from modes which could not be identified correctly or do not reflect the dynamic

damping model	Wing	Fuselage
RAYLEIGH	$g_{m,v} = 0.14$ $g_{s,v} = 3.81\text{e-}6$	$g_{m,v} = 1.92$ $g_{s,v} = 7.55\text{e-}6$
stiffness prop. structural	$g_{s,s} = 0.0054$	$g_{s,s} = 0.012$

TAB 4. Fitted loss factors g

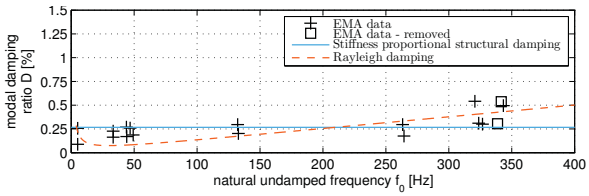

FIG 7. Loss factor g estimates: wing

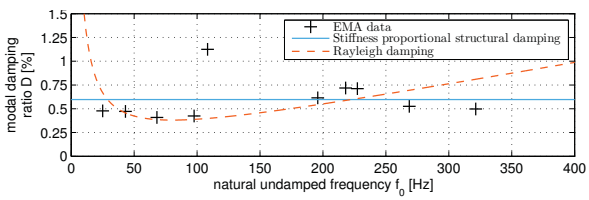

FIG 8. Loss factor g estimates: fuselage

behaviour of the structure but rather of the fixture were not included in this process.

The estimated values for the two damping models are listed in TAB. 4. The respective damping patterns are displayed in FIG. 7 and FIG. 8. For the wing, both models are good estimates due to low damping ratio scattering. For the fuselage, neither of the two modelling approaches are adequate to reflect all modal damping ratios.

In case of modal damping, the generalised substructure damping matrices $[D_{gen}]$ or $[C_{gen}]$ are constructed, each according to EQ. (8) and EQ. (10) with the help of the analytical substructure FE modal properties and the identified modal damping ratios D_h. In order to achieve substructure damping matrices $[D]$ and $[C]$, a modal synthesis according to EQ. (9) and EQ. (11) is required.

In a following step, the calculated substructure damping matrices are appropriately coupled for all four cases of damping models to construct a nonproportional, uncondensed system damping matrix of the full test bed structure AIRMOD. The system damping matrix has the following structure for all cases.

$$[D] = \begin{bmatrix} [D_{wing}] & [0] \\ [0] & [D_{fuselage}] \end{bmatrix} \text{ or } \quad [C] = \begin{bmatrix} [C_{wing}] & [0] \\ [0] & [C_{fuselage}] \end{bmatrix} \tag{13}$$

For both modal damping models, under the circumstances as in EQ. (13), the solution of the MDOF equations of motion must lead to *equivalent* damping ratios and equal behaviour at resonance peaks.

With the full structure uncondensed system matrices at hand, damping included, the uncondensed equations of motions for the full structure are set up. They are used to formulate the quadratic damped eigenvalue problem.

In case of the stiffness proportional structural damping, the system matrices $[K^c]$ and $[M]$ are well-conditioned, in accordance with statements in [1], and the problem yields stable solutions. In case of RAYLEIGH damping, the system matrices $[A]$ and $[B]$ are not well conditioned and require modal condensation for stable solutions. In case of modal damping, the system matrices are badly conditioned and require modal condensation for improved solution stability. Further approximations as in [1] are avoided to get the most accurate results.

A residual sum of squares Z is calculated on the basis of the correlated modal damping ratio differences $\varepsilon = D_{h,EMA} - D_{h,FE}$ of the elastic modes, with a weighting matrix $[W_\varepsilon]$ according to the confidence in the experimental results.

$$Z = \{\varepsilon\}^\mathsf{T}[W_\varepsilon]\{\varepsilon\} \tag{14}$$

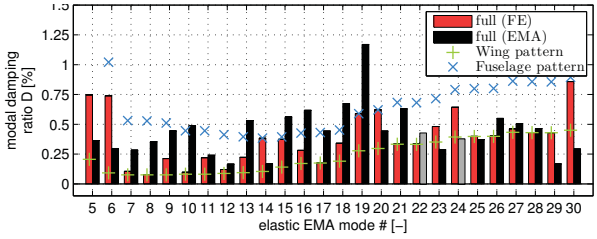

FIG 9. Coupling results: RAYLEIGH damping ($Z = 2.03 \times 10^{-4}$)

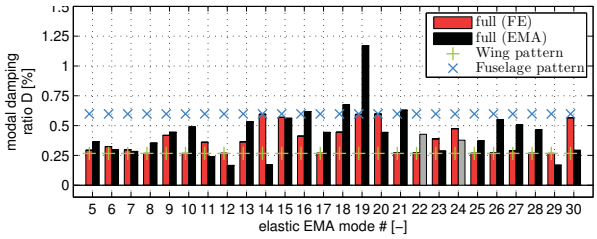

FIG 10. Coupling results: Stiffness proportional structural damping ($Z = 1.17 \times 10^{-4}$)

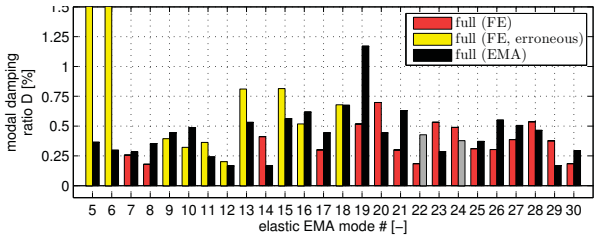

FIG 11. Coupling results: Modal damping (Z not applicable due to erroneous results)

4.1 RAYLEIGH damping

FIG. 9 shows the results of the eigenvalue problem regarding RAYLEIGH damping. The predicted modal damping ratios of the elastic modes are displayed in red bars next to the correlated, experimentally identified modal damping ratios for the full structure in black bars for mode per mode comparison. Grey bars indicate experimental results with a low confidence level. The damping ratios of the fuselage and the wing for the respective estimates at the same frequency are shown as plus markers. The chart shows that all predicted modal damping ratios lie between the substructure estimates. Each of them is closer to the estimate of the substructure which is involved stronger in the mode shape. Altogether, the predictions are of an insufficient quality and do not reflect the damping pattern of the assembled structure.

4.2 Stiffness proportional structural damping

FIG. 10 shows the results regarding stiffness proportional structural damping, in the same way as FIG. 9. Here also, all predicted predicted modal damping ratios lie between the substructure estimates. The modal damping ratios of most modes are better predicted,

especially the low-frequency elastic wing-only modes. This observation is supported by a comparison of the residual sum of squares Z, shown in the caption. However, experimental damping ratios of modes with elastic fuselage displacement poorly match with calculated results.

4.3 Modal damping

FIG. 11 shows the results regarding modal damping. Bars in red represent predicted FE results which are the same for viscous and modal damping. Bars in yellow represent predicted results which are different for both modal damping models. These results are suspected to suffer from numerical error for both modal damping applications, because the calculated rigid body modes showed too high modal frequencies and extremely unphysical modal damping ratios in both cases, despite modal condensation. This probably influenced the modes in yellow, because they are exactly those modes which exhibit considerable bungee strain. Yet, even when only the valid results are considered, the prediction quality is not significantly better than for the other models.

4.4 Preliminary Assessment

The prediction results are unsatisfactory. Modal damping, although reproducing substructure damping very well, suffers from an unphysical approach, fully populated matrices and bad matrix conditioning. RAYLEIGH viscous and stiffness proportional structural damping lead to comprehensible results, but these results do not reflect the full structure damping pattern due to the limited damping modelling capacity on substructure level, especially for the fuselage.

5. UPDATING SYSTEM DAMPING PARAMETERS

One approach to improve the damping modelling on substructure level is the further separation of the substructures into their individual components. These components shall have proportional damping matrices which are dependent on the component and loss factors g. Coupling these component damping matrices shall lead to non-proportional substructure damping matrices which should improve the agreement between the experimentally identified modal damping ratios and the correlated analytically calculated modal damping ratios due to more damping parameters and improved damping localisation. In the end, the improved damping modelling of the substructures shall also lead to a better prediction of the overall damping pattern of the full structure after a coupling process.

For this task, computational model updating (CMU) will be applied to adjust the FE component damping parameters governing the substructure damping matrix in order to improve the agreement of analytical and experimental results. It is based on the minimisation of an objective function Z which is a sum of squared residuals as in EQ. (14).

The mathematical theory for the CMU of damped systems must first be developed and then checked on an arbitrary, simulated structure to evaluate its suitability before it can be applied on real structures like AIRMOD.

5.1 Theoretical Background

The sensitivity method is the most common and most successful method to the problem of updating FE models of engineering structures based on vibration test data. It is based upon linearization of the generally non-linear relationship between experimental results, such as natural frequencies and mode shapes, and the parameters of the model in need of correction.

For example, the non-linear relationship of the j-th output of the analytical model $z_{a,j}$ on the k-th system parameter p_k can be developed from a TAYLOR series expansion truncated after the linear term at $p_k = p_{k,0}$

$$z_{a,j}(p_k) \approx z_{a,j}(p_{k,0}) + \left.\frac{\partial z_{a,j}}{\partial p_k}\right|_0 (p_k - p_{k,0}) \tag{15}$$

If the error $\nu_j = z_{m,j} - z_{a,j}(p_k)$ and the residual $\varepsilon_j = z_{m,j} - z_{a,j}(p_{k,0})$ are introduced as the difference between the measured output $z_{m,j}$ and the corresponding calculated output $z_{a,j}$ at p_k or $p_{k,0}$ respectively, EQ. (15) can be transformed to

$$\varepsilon_j = \nu_j + \left.\frac{\partial z_{a,j}}{\partial p_k}\right|_0 \Delta p_k \tag{16}$$

An equation system can be established

$$\begin{Bmatrix} \varepsilon_1 - \nu_1 \\ \vdots \\ \varepsilon_j - \nu_j \end{Bmatrix} = \left[\begin{matrix} \frac{\partial z_{a,1}}{\partial p_1} & \dots & \frac{\partial z_{a,1}}{\partial p_k} \\ \vdots & \vdots & \vdots \\ \frac{\partial z_{a,j}}{\partial p_1} & \dots & \frac{\partial z_{a,j}}{\partial p_k} \end{matrix}\right]_{p=p_0} \begin{Bmatrix} \Delta p_1 \\ \vdots \\ \Delta p_k \end{Bmatrix} = [G_z]\{\Delta p\} \tag{17}$$

where $[G_z]$ is a first-order sensitivity matrix. If $[G_z]$ has full rank and is invertible, the equation system can be solved by linear least squares for the parameter changes $\{\Delta p\}$ which are then used to update the parameters $\{p\}$ for a next iteration.

For the problem at hand, relevant outputs z_j are the complex eigenvalues λ_j of the elastic modes. The analytical formulation in [9] to calculate eigenvalue sensitivity is valid only for undamped systems and cannot be employed here. Instead, the complex eigenvalue sensitivity for viscously damped systems, developed and studied in [2], must be used.

$$\frac{\partial \lambda_j}{\partial p_k} = \lambda_j \frac{\{\psi_j\}^{\mathsf{T}} \left(\frac{\partial [K]}{\partial p_k} + \lambda_j^2 \frac{\partial [M]}{\partial p_k} + \lambda_j \frac{\partial [D]}{\partial p_k} \right) \{\psi_j\}}{\{\psi_j\}^{\mathsf{T}} \left(-\lambda_j^2 [M] + [K] \right) \{\psi_j\}} \tag{18}$$

The derivation of a formulation for structurally damped systems can also be achieved with EQ. (7) as fun-

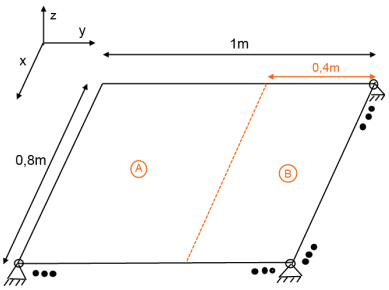

FIG 12. Plate - Sketch with dimensions

damping model	A	B
RAYLEIGH	$g_{m,v,A} = 28.19$ $g_{s,v,A} = 2.11\text{e-}5$	$g_{m,v,B} = 35.24$ $g_{s,v,B} = 2.64\text{e-}5$
stiffness prop. structural	$g_{s,s,A} = 0.08$	$g_{s,s,B} = 0.1$

TAB 5. Example loss factors g

damental assumption. Then, the derivation succeeds in the very same way as the derivation for EQ. (18) presented in [2].

$$\frac{\partial \lambda_j}{\partial p_k} = \lambda_j \frac{\{\psi_j\}^\intercal \left(\frac{\partial [K^c]}{\partial p_k} + \lambda_j^2 \frac{\partial [M]}{\partial p_k} \right) \{\psi_j\}}{\{\psi_j\}^\intercal \left(-\lambda_j^2 [M] + [K^c] \right) \{\psi_j\}} \tag{19}$$

5.2 Example

Instead of AIRMOD, the numerical test case consists of a linear elastic, stiff, thin rectangle plate, simply supported along all sides. It has side lengths of 0.8 m and 1.0 m, is 0.01 m thick and consists of homogenous isotropic aluminum. In addition, this plate is subdivided into two firmly connected plate components A and B which have the dimensions shown in FIG. 12.

It is modelled according to the KIRCHHOFF theory. The NASTRAN FE model consists of 32 times 40 square CQUAD4 plate elements and has 6527 nodes. Its mesh is converged for the first 10 modes. In a following step, the a-set stiffness and mass matrices are exported from NASTRAN and imported to MATLAB.

5.3 Sensitivity Analysis

Relevant inputs p for the problem of adjusting the FE substructure modal damping ratios are component loss factors g. Therefore, arbitrarily chosen loss factors g, listed in TAB. 5, are first assigned to the plate components according to the damping model. In each case, the solution of the eigenvalue problem of the damped system leads to j complex pairs of eigenvalues λ_j and complex eigenvectors $\{\psi_j\}$.

Sensitivities are then calculated. Because loss factors do not have an influence on the mass and stiffness properties of a structure, EQ. (18) and EQ. (19) can be simplified.

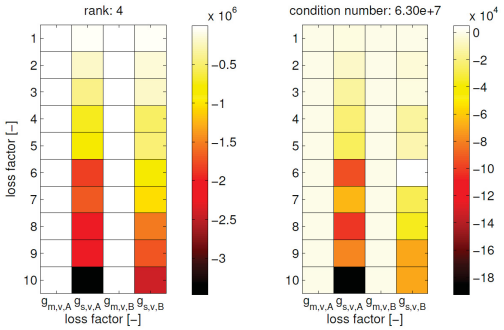

FIG 13. Sensitivity matrix $[G_\lambda]$, split into real and imaginary part: RAYLEIGH damping

$$\frac{\partial \lambda_j}{\partial g_k} = \lambda_j \frac{\{\psi_j\}^\intercal \left(\lambda_j \frac{\partial [D]}{\partial g_k} \right) \{\psi_j\}}{\{\psi_j\}^\intercal \left(-\lambda_j^2 [M] + [K] \right) \{\psi_j\}} \tag{20}$$

$$\frac{\partial \lambda_j}{\partial g_k} = \lambda_j \frac{\{\psi_j\}^\intercal \left(\frac{\partial [C]}{\partial g_k} \right) \{\psi_j\}}{\{\psi_j\}^\intercal \left(-\lambda_j^2 [M] + [K^c] \right) \{\psi_j\}} \tag{21}$$

The derivatives of the damping matrices $\frac{\partial [D]}{\partial g_k}$ and $\frac{\partial [C]}{\partial g_k}$ are calculated by finite differences. This means, a small fraction $\partial g_k = 0.01\% g_k$ is added to the original value of the loss factor g_k and the difference between the original and the new damping matrix is calculated.

The calculated complex sensitivity matrix $[G_\lambda]$ regarding RAYLEIGH damping is shown in FIG. 13 in a coloured pattern for the first 10 modes, split into real and imaginary part. It was calculated with the eigenvalues with a positive imaginary part and the corresponding eigenvector only. It shows that growing loss factors g_k lead to a growth of D and a drop of the damped natural frequency. Generally, $\Re(\lambda_k)$ displays a stronger sensitivity to changes of loss factors g for the larger and heavier plate section A than for B which is reasonable. The complex sensitivity matrix for stiffness proportional structural damping reveals equivalent results.

Both sensitivity matrices have full rank and can therefore be inverted and used for computational model updating. The condition numbers for each matrix are low enough for this example to guarantee an almost lossless numerical inversion.

5.4 Consistent and inconsistent error cases

The updating procedure is iterative and starts at $q = 0$ with a set of loss factors $g_{q=0}$ which result into eigenvalues λ_q and eigenvectors $\{\psi\}_q$. With this information, a complex sensitivity matrix $[G_{\lambda,q}]$ can be calculated. The distance of the target eigenvalues λ_m to the corresponding λ_q makes up the vector of complex residuals $\{\varepsilon\}_q = \{\lambda_m\} - \{\lambda_q\}$ which is needed for the equation system and complex objective function Z_λ.

Both, residuals and elements of the sensitivity matrix are weighted with the absolute target eigenvalue $|\lambda_m|$. Finally, EQ. (17) is solved by weighted linear least

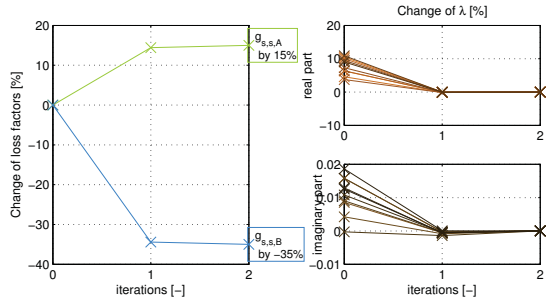

FIG 14. Consistent test case: stiffness proportional structural damping

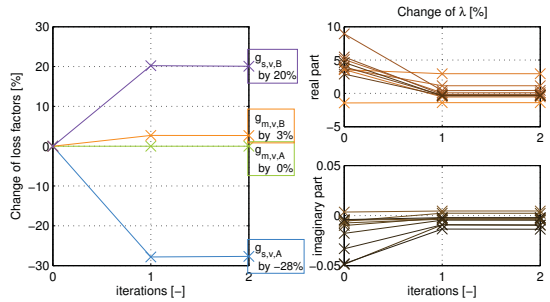

FIG 15. Inconsistent test case: RAYLEIGH damping

squares. The solution $\{\Delta g\}$ is weakly complex such that its real part is a good approximation to update the loss factors $\{g\}_{q=1} = \{g\}_{q=0} + \Re(\{\Delta g\})$.

For the consistent error test case, the difference to the simulated target eigenvalues $\{\lambda_m\}$ is only dependent on the loss factors g. Therefore, arbitrary errors are added on a chosen set of loss factors starting values $g_{q=0}$ and target eigenvalues are calculated. In this case for structural damping, +15% were added on $g_{s,s,A}$ and -35% were put on $g_{s,s,B}$ from TAB. 5.

The results are shown in FIG. 14. Within two iterations, the starting values of the loss factors change by the chosen error percentage and all of the complex system eigenvalues approach the target eigenvalues very closely so that the iteration is stopped.

The inconsistent error case is quite similar to the consistent test case. In this case for RAYLEIGH damping, +15% were put on $g_{m,v,A}$, -35% on $g_{s,v,A}$, -20% on $g_{m,v,B}$ and +30% on $g_{s,v,B}$. But this time, the loss factor $g_{m,v,A}$ is excluded from updating.

The results are shown in FIG. 15. After already two iterations, the loss factors converge, indicating the stability of the approach with respect to inconsistent updating cases. The unblocked loss factors change in such a way that the complex objective function Z_λ is minimal. The deviation of the eigenvalues from the target eigenvalues drops visibly.

6. CONCLUSION

The numerical prediction quality of modal damping properties of assembled structures with proportionally damped substructures was assessed for different damping models on the basis of experimental results. It was shown in section 4 on behalf of the AIRMOD structure that the application of stiffness proportional structural damping leads to the best predictive results, although the substructure damping pattern is approximated only very roughly with this model. However, even these results are unsatisfactory and show that proportional damping models on substructure level cannot sufficiently describe the full structure damping pattern.

Therefore, a computational model updating approach on the basis of complex eigenvalue sensitivity was introduced in section 5 in order to adjust loss factors of substructure components. It was successfully checked on a numerical test case with consistent and inconsistent errors for stiffness proportional structural and RAYLEIGH damping models. For future use, this approach must be reviewed, checked on the AIRMOD and further matured for applications to real structures.

REFERENCES

[1] A. Rittweger, S. Dieker, K. Abdoly, and J. Albus. Coupled Dynamic Load Analysis with different Component Damping of the Substructures. In *Proceedings of the 59th International Astronautical Congress*, volume 8, pages 5386–5398. International Astronautical Federation, 2008.

[2] S. Adhikari. Rates of Change of Eigenvalues and Eigenvectors in Damped Dynamic Systems. *AIAA Journal*, 39(11):1452–1457, 1999.

[3] E. Balmès. GARTEUR Group on Ground Vibration Testing. Results from the Test of a Single Structure by 12 Laboratories in Europe. In *Proceedings of the International Modal Analysis Conference*, 1997.

[4] M. Degener. Ground Vibration Tests on an Aircraft Model Performed as Part of a European Round Robin Exercise. In *Proceedings of the International Forum on Aeroelasticity and Structural Dynamics*, 1997.

[5] Y. Govers. *Parameter Identification of Structural Dynamic Models by Inverse Statistical Analysis*. Research report, Deutsches Zentrum für Luft- und Raumfahrt e.V., Göttingen, 2012.

[6] Y. Govers et al. A Comparison of two Stochastic Model Updating Methods Using the DLR AIRMOD Test Structure. *Mechanical Systems and Signal Processing*, 52-53:105–114, 2015.

[7] P. Guillaume et al. A Poly-Reference Implementation of the Least-Squares Complex Frequency-Domain Estimator. In *Proceedings of the 21st International Modal Analysis Conference*, pages 183–192, 2003.

[8] R. J. Allemang and D. L. Brown. A Correlation Coefficient for Modal Vector Analysis. In *Proceedings of the 1st International Modal Analysis Conference*, pages 110–116, 1982.

[9] R. L. Fox and M. P. Kapoor. Rates of Change of Eigenvalues and Eigenvectors. *AIAA Journal*, 6(12):2426–2429, 1968.